Title

Osteoprotegerin-eluting nanoparticulate mineralized collagen scaffolds improve skull regeneration.

Authors

Ren, Xiaoyan
Dejam, Dillon
Oberoi, Michelle
et al.

Publication Date

2023-02-01

DOI

10.1016/j.bioadv.2022.213262

Peer reviewed

HHS Public Access

Author manuscript

Biomater Adv. Author manuscript; available in PMC 2024 February 01.

Published in final edited form as:

Biomater Adv. 2023 February ; 145: 213262. doi:10.1016/j.bioadv.2022.213262.

Osteoprotegerin-Eluting Nanoparticulate Mineralized Collagen Scaffolds Improve Skull Regeneration

Xiaoyan Ren[1], **Dillon Dejam**[1], **Michelle K. Oberoi**[1], **Natalie J. Dahan**[1], **Qi Zhou**[1], **Kelly X. Huang**[1], **Meiwand Bedar**[1], **Candace H. Chan**[1], **Vasiliki Kolliopoulos**[2,3], **Marley J. Dewey**[2], **Brendan A.C. Harley**[2,3], **Justine C. Lee**[1,4,5,6,*]

[1]Division of Plastic and Reconstructive Surgery, UCLA David Geffen School of Medicine, Los Angeles, CA 90095 and Greater Los Angeles VA Healthcare System, Los Angeles, CA 90073

[2]Department of Chemical and Biomolecular Engineering, University of Illinois at Urbana-Champaign, Urbana, IL 61801

[3]Carl R. Woese Institute for Genomic Biology, University of Illinois at Urbana-Champaign, Urbana, IL 61801

[4]UCLA Molecular Biology Institute, Los Angeles, CA 90095

[5]Department of Orthopaedic Surgery, UCLA David Geffen School of Medicine, Los Angeles, CA 90095

[6]Research Service, Greater Los Angeles Veterans Affairs Healthcare System, Los Angeles, CA 90073

Abstract

Custom synthesis of extracellular matrix (ECM)-inspired materials for condition-specific reconstruction has emerged as a potentially translatable regenerative strategy. In skull defect reconstruction, nanoparticulate mineralized collagen glycosaminoglycan scaffolds (MC-GAG) have demonstrated osteogenic and anti-osteoclastogenic properties, culminating in the ability to partially heal *in vivo* skull defects without the addition of exogenous growth factors or progenitor cell loading. In an effort to reduce catabolism during early skull regeneration, we fabricated a composite material (MCGO) of MC-GAG and recombinant osteoprotegerin (OPG), an endogenous anti-osteoclastogenic decoy receptor. In the presence of differentiating osteoprogenitors, MCGO demonstrated an additive effect with endogenous OPG limited to the first 14 days of culture with total eluted and scaffold-bound OPG exceeding that of MC-GAG. Functionally, MCGO exhibited similar osteogenic properties as MC-GAG, however, MCGO significantly reduced maturation and resorptive activities of primary human osteoclasts. In a rabbit skull defect model, MCGO scaffold-reconstructed defects displayed higher mineralization as well as increased hardness and microfracture resistance compared to non-OPG functionalized MC-GAG scaffolds. The current work suggests that MCGO is a development in the goal of reaching a materials-based strategy for skull regeneration.

*corresponding author: justine@ucla.edu.

Patents: The material presented is the subject of USPTO PCT/US2019/016709 and USPTO PCT/US2022/041269.

Conflict of Interest Disclosures: JCL is a medical education consultant for Stryker.

Introduction

Approximately 13.8 million procedures that enter the cranial vault are performed annually worldwide for trauma, cancer, cerebrovascular disease, and congenital anomalies [1]. Reconstruction of the skull is necessary and routine for the purposes of cerebral protection, normal neurologic functioning, as well as psychological and vocational functioning [2–4]. While the first-line treatment for cranial defects is replacement of the autologous orthotopic bone, circumstances such as tumor invasion or contamination necessitate the usage of alternative autologous or alloplastic materials for reconstruction, both of which have inherent drawbacks. The former is limited by size and donor site morbidity and the latter has been well associated with higher infectious risks [5–7]. The distinct shortcomings of autologous bone harvest and clinically available alloplastic substances have opened opportunities for regenerative approaches for skull reconstruction.

The ability of the extracellular matrix (ECM) to coordinate differential cell fates in multicellular systems to generate summary responses has suggested the potential for translating ECM-inspired regenerative materials [8, 9]. In synthetic ECM-inspired materials, the added dimension of customizability suggests the development of condition-specific regeneration, optimized beyond solely tissue type to the anatomic, biomechanical, and functional requirements of the clinical scenario. Previously, we reported that a novel, synthetic material composed of nanoparticulate mineralized collagen glycosaminoglycan (MC-GAG) scaffold could partially regenerate *in vivo* skull defects without progenitor cell seeding or addition of exogenous growth factors [10–15]. Mechanistically, MC-GAG scaffolds demonstrated the ability to induce osteogenic differentiation of primary human mesenchymal stem cells (hMSCs) via upregulation of the canonical bone morphogenetic protein receptor (BMPR) signaling pathway [11, 16]. One of the triggers for the osteogenic abilities of MC-GAG scaffold was a specific range of stiffness, while softer versions of MC-GAG displayed reduced mineralization [17, 18].

Separate from its osteogenic capabilities, MC-GAG also influenced osteoclast activation and maturation directly and indirectly [19, 20]. Immature osteoclast cultures with MC-GAG scaffolds displayed reduced maturation and resorption which could be further augmented by the stimulation of endogenous osteoprotegerin (OPG) expression from differentiating hMSCs in the scaffolds [19, 20].

The receptor activator of nuclear factor-κB (RANK), RANK ligand (RANKL), and OPG is essential to osteoclast regulation and bone homeostasis [21–24]. Binding of RANK to its ligand RANKL activates osteoclasts, whereas OPG serves to sequester RANKL from RANK (Figure 1A). While the absence of RANK or RANKL in mouse knockout models have resulted in a complete absence of osteoclasts, OPG knockouts exhibit overactive osteoclasts with severe osteoporosis [25, 26]. Augmentation of the indirect effect of MC-GAG scaffolds on osteoclast inhibition using adenoviral overexpression of OPG in hMSCs demonstrated that OPG did not affect osteogenic differentiation while the resorptive activities of osteoclasts were markedly reduced [20]. These data suggested that a MC-GAG and OPG composite material (MCGO) may potentially be a functional refinement towards

the ultimate goal of delivering a cell-free, materials-based regenerative strategy in skull reconstruction. To this end, the current work describes the fabrication, *in vitro*, and *in vivo* testing of MCGO.

Materials and Methods

Scaffold Fabrication

Non-mineralized glycosaminoglycan (Col-GAG) and MC-GAG scaffolds were prepared using a previously described lyophilization process [27–29]. Briefly, a suspension of collagen and GAGs was produced by combining microfibrillar, type I collagen (Collagen Matrix, Oakland, NJ) and chondroitin sulfate sodium (Spectrum Chemical Manufacturing Corporation, New Brunswick. NJ) with (MC-GAG) or without (Col-GAG) calcium salts (calcium nitrate hydrate: Ca(NO3)2·4H2O; calcium hydroxide: Ca(OH)2, Sigma-Aldrich, St. Louis, MO) in a solution of acetic acid (Col-GAG) or phosphoric acid (MC-GAG). The suspension was frozen using a constant cooling rate of 1°C/min from room temperature to a final freezing temperature of −10°C using a freeze dryer (Genesis, VirTis). Following sublimation of the ice phase, scaffolds were sterilized with ethylene oxide and cut into discs 4 mm in height and either 8 mm in diameter (*in vitro*) or 14 mm in diameter (*in vivo*). After rehydration with phosphate-buffered saline (PBS) overnight, crosslinking of scaffolds was performed in PBS using 1-ethyl-3-(3-dimethylaminopropyl)carbodiimide (EDAC; Sigma-Aldrich) and N-hydroxysuccinimide (NHS; Sigma-Aldrich) at a molar ratio of 5:2:1 (EDAC:NHS:COOH), where COOH represents the amount of collagen in the scaffold [30]. Composite OPG-eluting materials were fabricated by immersing scaffolds in 2 μg/mL of purified recombinant OPG (Peprotech, Rocky Hill, NJ) in PBS for 24-48 hours to generate CGO and MCGO scaffolds (Figure 1B) in a manner similar to that described by Tiffany et al [31].

Cell Culture

Primary hMSCs (Lonza, Allendale, NJ) were allowed to proliferate in medium comprised of Dulbecco's modified Eagle's medium (DMEM; Corning Cellgro, Manassas, VA) supplemented with 10% fetal bovine serum (FBS; Atlanta Biologicals, Atlanta, GA), 2 mM L-glutamine (Life Technologies, Carlsbad, CA), and 100 IU/mL penicillin/100 μg/mL streptomycin (Life Technologies). $3x10^5$ hMSCs were seeded onto 8 mm scaffolds and cultured in growth medium to the specified timepoints. For hMSC and primary human osteoclast (hOC) co-cultures, 6×10^4 hOCs were cultured in Osteoclast Precursor Basal Medium (Lonza, Allendale NJ) supplemented with 33 ng/mL M-CSF and 66 ng/mL RANKL on 24 well OsteoAssay Microplates. 24 h after hOCs were seeded, scaffolds were transferred to the OsteoAssay plates for direct co-cultures with hOCs in combined osteogenic and osteoclastogenic medium (Osteoclast Precursor Basal Medium supplemented with 33 ng/mL M-CSF, 66 ng/mL RANKL, 10 mM β-glycerophosphate, 50 μg/mL ascorbic acid, and 0.1 μM dexamethasone). Media were changed every 3 days for 2 weeks.

Enzyme Linked Immunosorbent Assay

Enzyme-linked immunosorbent assays (ELISA) were performed to determine concentrations of soluble OPG and RANKL. Protein concentrations were determined using the Human

OPG DuoSet and Human RANKL DuoSet ELISA kits (R&D Systems, Minneapolis, MN) according to manufacturer's instructions. Briefly, a 96 well microplate was coated with the capture antibody and incubated overnight at room temperature. After blocking, samples were incubated for 2 h at room temperature with the detection antibody followed by incubation with streptavidin-horseradish peroxidase for 20 min. The reaction was quenched with 2N H_2SO_4. Plates were read at 450 and 540 nm wavelengths on the Epoch Microplate Reader (BioTex, Winooski, VT).

Co-Immunoprecipitation

8 mm in diameter CGO or MCGO scaffold were incubated with 120 ng of purified RANKL (R&D Systems) in 1 mL of PBS with 1 mM EDTA overnight at room temperature. After washing scaffolds, protein extracts were prepared by morselizing the scaffolds in 500 μL RIPA buffer (Alfa Aesar, Ward Hill, MA). Lysates were then incubated with SureBeads Protein A Magnetic Beads (BioRad, Hercules, CA) with either rabbit anti-OPG (AbCam, Waltham, MA) or anti-RANKL (Cell Signaling Technology, Danvers, MA) at 4 °C overnight. Beads were washed and protein was eluted from beads by resuspending in 40 μL of sodium dodecyl sulfate (SDS) sample buffer and incubating at 70 °C for 10 minutes. The beads were then pelleted and the supernatant was loaded into SDS-PAGE gels for Western Blot analysis.

Western Blot

Total protein lysates were prepared by morselizing scaffolds using scissors in 3X SDS sample buffer, followed by incubation at 95 °C for 5 minutes. Lysates were then centrifuged in 0.2 μm Spin-X filters (Corning Costar, Corning, NY) at 14,000 rpm for 5 minutes. Following measurement of protein concentration, equal amounts were loaded onto 4 to 20% polyacrylamide gels in both reducing and nonreducing conditions (Bio-Rad, Hercules, CA) for electrophoresis and subsequent transfer onto a nitrocellulose membrane. Western blot analysis for OPG was performed using anti-OPG antibody (Santa Cruz Biotechnology, Santa Cruz, CA) followed by application of a 1:4000 dilution of HRP-conjugated anti-immunoglobulin G secondary antibody (Bio-Rad, Hercules, CA) and subsequent application of chemiluminescent substrate (Thermo Fisher Scientific, Rockford, IL).

Quantitative real-time reverse-transcriptase polymerase chain reaction

RNeasy kit (Qiagen, Valencia, CA) was used to extract total RNA from scaffolds at 7 days of culture. Gene sequences for 18S, OPG, RANKL, alkaline phosphatase (ALP), collagen 1A1 (COL1A1), osteocalcin (OCN), bone sialoprotein 2 (BSP2), runt-related transcription factor 2 (Runx2), BMP2, BMP4, BMP7, sex determining region Y-related high-mobility group box 9 (SOX9), collagen 2A1 (COL2A1), and collagen 10A1 (COL10A1) were obtained from the National Center for Biotechnology Information gene database and primers were designed (Supplementary Table 1). Quantitative real-time reverse-transcriptase polymerase chain reactions (QPCR) were performed on the Opticon Continuous Fluorescence System (Bio-Rad Laboratories, Inc., Hercules, CA) using the QuantiTect SYBR Green RT-PCR kit (Qiagen). Cycle conditions were as follows: reverse transcription at 50 °C (30 min); activation of HotStarTaq DNA polymerase/inactivation of

reverse transcriptase at 95 °C (15 min); and 45 cycles of 94 °C for 15 s, 58 °C for 30 s, and 72 °C for 45 s.

Immunofluorescent and Confocal Microscopy

For *in vitro* osteoclast cultures, 8 mm scaffolds were co-cultured with primary human osteoclasts on chamber slides (Lab-Tek, ThermoFisher, Waltham, MA) for 14 days as described above. Scaffolds were then removed from the chamber slides and slides were fixed with 4% paraformaldehyde. Slides were then blocked and permeabilized with PBS-Triton 0.02% plus 10% normal goat serum (Jackson ImmunoResearch Laboratories, West Grove, PA) for 1 hour and subjected to heat-induced antigen retrieval using sodium citrate buffer (10 mM, pH 6) at >80°C, for 20 minutes. Slides were then incubated with anti-TRAP (AbCam, Waltham, MA; 1:100) overnight at room temperature. After washing, slides were incubated in anti-mouse IgG Alexa Fluor Plus 594 (Cell Signaling Technology, Danvers, MA; 1:1000) for 4 hours. After washing again, slides incubated with Alexa Fluor ® 488 phalloidin (Cell Signaling Technology, Danvers, MA, 1:50) to label actin for 45 minutes. Slides were then washed and incubated with Dapi (Cell Signaling Technology, Danvers, MA; 1:1000) for 10 min. Coverslips were mounted with Prolong Gold Antifade Reagent (Cell Signaling Technologies, Danvers, MA). Images were captured with the Zeiss Axio Observer 3 inverted microscope with the ZEN 2.3 Pro software (Zeiss, Oberkochen, Germany) and the Zeis LSM900 confocal laser scanning microscope with Zen 3.1 Blue software (Zeiss, Oberkochen, Germany).

WST-1 Assay

Cellular proliferation reagent WST-1 (Roche, Basel, Switzerland) was supplemented to culture medium at a concentration of 1:10, followed by incubation for 3 to 4 hours at 37 °C in a humidified atmosphere with 5% CO_2. Absorbance at 450 nm and 690 nm was then measured (Epoch, BioTek, Winooski, VT).

Micro-Computed Tomography

Scaffolds were fixed in a solution of 10% formalin for 24 hours and subsequently stored in 70% ethanol at 4 °C until imaging was performed using the Scanco μCT 35 (Scanco Medical AG, Bruttisellen, Switzerland). Scaffolds were wetted with PBS prior to scanning and placed directly onto the scanner's sample holder and imaged using medium resolution settings, with a source voltage E of 70 kVp, current I of 114 μA, and a voxel size of 12.5 μm. Scaffold areas were contoured to establish volumes of interest for quantification of mineralization, and optimum arbitrary threshold values of 20 (showing scaffold and mineralization) and 80 (mineralization alone) were used to distinguish true mineralization from unmineralized scaffold. Analysis of three-dimensional reconstructions was performed using Scanco Evaluation script no. 2 (3D segmentation of two volumes of interest: solid dense in transparent low-density object) and script no. 6 (bone volume/density-only bone evaluation). Scans were then exported for subsequent analyses using ImageJ [32]. For analysis, heterogeneity among the *in vivo* micro-CTs were accounted for by delineating a specific volume for comparison as well as a correction factor using native bone. For each slice of the scan, a 3 mm (native bone) or 12 mm (defect) in diameter circular selection was made and a macro was used to measure the mean gray value for each area. All slices with

negative mean gray values were excluded. For each of the remaining slices, the median of the mean gray values was calculated and 40 slices in total centered on the median were used for the final analysis. For the native bone, an average of the 40 slices served as the internal control and the correction factor for the defect. Each of the mean gray values within the 40 slices of the defect were then divided by the correction factor for each individual animal resulting in the final value of Defect/Native Mineralization.

Resorption Pit Assay

Evaluation of OC resorption activity was evaluated on OsteoAssay plates in culture. Following aspiration of culture medium, 500 μL of 10% bleach was added and incubated for 5 minutes at room temperature. After washing with distilled water, wells were dried at room temperature for 3-5 hours. Pits were imaged using light microscopy at a magnification of 2.5X. Areas of resorption were analyzed using ImageJ (NIH, Bethesda, MD).[32]

Rabbit Calvarial Defect Implantation

New Zealand white rabbits were divided into 3 groups by implant: Defect only (negative control), MC-GAG, and MCGO. Following induction of anesthesia, the scalp was incised and pericranium was dissected away from the calvarium. 14 mm biparietal defects were created in each rabbit using a hand-powered trephine and the bone was carefully lifted. For rabbits within the negative control, Defect only group, the skin was then closed with 4-0 nylon sutures without reconstruction of the defect. For rabbits in the MC-GAG and MCGO groups, 14 mm corresponding scaffolds were placed into the defect and the incision was then closed with 4-0 nylon sutures. Twelve weeks after defect creation and scaffold implantation, rabbits were euthanized and the calvarium including both the defect and surrounding native bone was explanted for analysis.

Histology and Quantification of Regenerated Bone

Explanted rabbit skulls were fixed in 10% formalin, embedded in paraffin, and sectioned at 4 microns using standard techniques. The sections were deparaffinized and stained with hematoxylin and eosin (H&E). Images of the junction between native bone and regenerated bone were photographed at 2-2.5X magnification in standard light microscopy. Quantitative analysis was carried out using ImageJ by assessing the ratio of the area of regenerated bone to the total defect area including bone and soft tissue.

Reference Point Indentation

Explanted rabbit skulls stored in 10% formalin were indented with the BioDent reference point indentation device (Active Life Scientific, Santa Barbara, CA) according to manufacturer's instructions. Indentations were conducted at a force of 2N, an indentation frequency of 2 Hz, and 10 indentation cycles at a touchdown force of 0.1 N using a probe assembly type BP2. Indentation data was analyzed with the BioDent software for the first cycle indentation distance (ID1st), total indentation distance (TID), unloading slopes (US), and loading slope (LS). Hardness, highly correlated to density and mineralization, is estimated by ID1st [33]. Toughness, or resistance to fracture, is inversely correlated to TID. Relative stiffness was determined by the US and LS of the force (N) to displacement

(μm) curves. For each skull, microindentations were performed in at least 20 different areas within the defect and 5 different areas within the native bone. To minimize differences in the thickness of bone for each animal as well as the bone healing capabilities, data from each cranial defect was internally controlled with the native calvarial bone.

Statistical Analyses

For the longitudinal OPG and RANKL ELISAs, two way repeated measures analyses of variance (ANOVA) were performed to examine the effects of scaffold type and time in culture on the respective protein concentrations. When a significant interaction was found, simple effects were used to compare the concentrations between scaffold type at each time point. Posthoc comparisons were performed with Bonferroni adjustments. Mean differences between *in vitro* microCT, WST-1 analyses, and resorption pit assays were compared with either a student's t test or a one-way ANOVA with posthoc comparisons under the Tukey criterion. Differences between molar ratios of OPG/RANKL, *in vivo* microCT, and reference point indentation analyses were compared with a Kruskal-Wallis test due to non-normal distributions of the data. Pairwise comparisons were performed using the Dunn's test with a Bonferroni adjustment. All statistical analyses were performed using GraphPad Prism (San Diego, CA) or SPSS Version 27 (Chicago, IL).

Results

MCGO OPG Elution in Cell-Free Scaffolds and in Combination with Endogenous OPG Secretion from hMSCs

To understand the OPG elution kinetics of MCGO over time, four analyses were carried out using two-way repeated measures ANOVA with posthoc comparisons using the Bonferroni criterion (Figure 2 and Supplementary Tables 2–4). Scaffold type and time were evaluated as the main effects while the interaction between scaffold type and time was also assessed. First, 8 mm cell-free CGO, as a control material, and MCGO scaffolds were cultured in growth media with changes every 3 days for 8 weeks, with OPG release characterized via ELISAs (Figure 2A). There was a significant main effect of scaffold type [$F(1,2)=111.85$, $p=0.009$] on OPG elution with an estimated marginal mean of 6.31 (95%CI 5.27-7.35) ng/mL for CGO and 8.25 (95%CI 7.76-8.74) ng/mL for MCGO. There was also a significant main effect of time [$F(8,16)=1606.90$, $p<0.001$] on OPG elution. There was also a significant interaction between the scaffold type and time on OPG elution [$F(8,16)=51.19$, $p<0.001$]. Simple effects to determine the differences between the scaffolds at each timepoint were then performed. Pairwise comparisons demonstrated that MCGO scaffolds eluted higher levels of OPG from day 7 to day 35. While differences were still present at day 56, the amount of additional OPG elution after day 35 was low.

Next, we evaluated endogenous OPG secretion using 8mm Col-GAG and MC-GAG materials cultured with 3×10^5 hMSCs in growth media over 8 weeks (Figure 2B). At the same intervals as the cell-free analysis, culture media was collected and assessed with ELISA for secreted OPG. Again, there was a significant main effect of scaffold type [$F(1,3)=50.17$, $p=0.006$] on endogenous OPG concentrations with an estimated marginal mean of 12.52 (95%CI 11.14-13.90) ng/mL for Col-GAG and 15.68 (95%CI 15.09-16.26)

ng/mL for MC-GAG, both are nearly twice as much as the corresponding cell-free CGO and MCGO scaffolds. There was also a significant main effect of time [$F(8,24)=234.84$, $p<0.001$] on OPG concentrations. There was also a significant interaction between the scaffold type and time on OPG elution [$F(8,24)=2.94$, $p=0.019$]. Pairwise comparisons demonstrated that hMSCs cultured on MC-GAG secreted higher levels of soluble OPG from day 0 to day 21 with differences between the scaffolds tapering thereafter. Unlike cell-free materials, endogenous secretion displayed an increase in OPG concentrations over time.

Next, we assessed the combination of endogenous OPG secretion and the OPG eluting scaffolds on total soluble OPG concentrations (Figure 2C). 3 x 10^5 hMSCs were cultured on 8 mm CGO and MCGO scaffolds for 8 weeks. Culture media was again collected over the same period as the same intervals as above for OPG ELISA. Similar to the previous models, there was a significant main effect of scaffold type [$F(1,3)=32.10$, $p=0.011$] on soluble OPG concentrations with an estimated marginal mean of 17.19 (95%CI 15.58-18.80) ng/mL for CGO and 21.21 (95%CI 20.54-21.87) ng/mL for MCGO. There was also a significant main effect of time [$F(8,24)=130.82$, $p<0.001$] and a significant interaction between the scaffold type and time on OPG elution [$F(8,24)=14.51$, $p<0.001$]. Early in culture at days 0 and 3, no significant differences were seen between the materials, similar to the cell-free CGO and MCGO elution patterns. Between days 7 and 28, an initial reduction followed by increase in soluble OPG was found in both scaffolds with MCGO demonstrating significantly higher quantities of soluble OPG. The differences tapered after day 28, albeit small but significant differences could be elicited between the scaffolds even at day 56.

Lastly, given that MC-GAG and MCGO are the primary materials of interest, the final model assessed the combination effect of OPG elution from the scaffold and endogenous OPG secretion from hMSCs cultured on MC-GAG and MCGO (Figure 2D). Significant main effects of scaffold type [$F(1,3)=1066.14$, $p<0.001$] and time [$F(8,24)=50.63$, $p<0.001$] were found on OPG concentrations. There was a significant interaction between scaffold type and time [$F(8,24)=126.45$, $p<0.001$]. On pairwise comparisons, the differences between MC-GAG and MCGO were specifically within the first 14 days of culture with no significant differences between days 21 and 42. Of note, the estimated marginal mean concentrations of OPG in the presence of the MCGO scaffold ranged between 22-25 ng/mL, similar to the soluble OPG concentrations found at day 56 with normal endogenous OPG secretion on MC-GAG. Taken together, these data suggest that MCGO elutes more OPG compared to CGO and generates a higher quantity of soluble OPG compared to the MC-GAG base material.

OPG/RANKL Expression Relationships and Protein Interactions Between Scaffold-bound OPG and RANKL

While the combination of MCGO-mediated OPG elution and endogenous OPG secretion results in higher quantities of OPG, the relative quantities and binding affinities of OPG to RANKL dictate the potential for osteoclast inhibition. To understand whether endogenous RANKL production is affected by the OPG-eluting scaffolds, RANKL ELISAs were also carried out over the same time period. Again, 3 x 10^5 hMSCs were cultured on conventional non-mineralized (Col-GAG) or mineralized (MC-GAG) collagen scaffolds or in the presence

of OPG-functionalized versions (CGO, MCGO) for 8 weeks (Figure 3). Unlike OPG, no significant differences were seen in RANKL concentrations among scaffold type or over time.

To understand the overall balance between OPG and RANKL, molar ratios were then evaluated over the initial 14 days of culture as the first 14 days were found to differentiate between MCGO and MC-GAG OPG concentrations (Figure 3C). Due to a non-normal distribution, OPG/RANKL molar ratios were compared using a Kruskal-Wallis test and found to exhibit significant differences among the scaffolds [$H(3)=16.10$, $p=0.001$]. MCGO generated significantly higher OPG/RANKL ratios compared to MC-GAG [median(IQR, interquartile range): 188.84(36.30) vs. 145.05(88.60), $p=0.004$]. For the purposes of comparison, Col-GAG and CGO were included in the analysis, albeit the differences in molar ratios between the Col-GAG and CGO did not reach statistical significance. MCGO scaffolds also trended towards a higher OPG/RANKL ratio compared to non-mineralized CGO scaffolds. In contrast to the differences in OPG protein quantities, gene expression of OPG was not significantly different among the four materials, suggesting that OPG-eluting scaffolds did not affect endogenous OPG expression (Figure 3D). RANKL expression was also largely similar among the different materials with slightly more expression in hMSCs cultured on Col-GAG scaffolds compared to MC-GAG (Figure 3E).

To confirm that the OPG eluted from MCGO scaffolds was a functional decoy receptor for RANKL, co-immunoprecipitation experiments were performed to assess binding capabilities (Figure 3F). Cell-free CGO and MCGO were incubated with purified RANKL protein and subjected to immunoprecipitation with either RANKL or OPG antibodies. In scaffold lysates, MCGO displayed higher quantities of OPG compared to CGO, corresponding to the higher quantities of eluted OPG seen on ELISA (Figure 2). The higher quantities of OPG also corresponded to a higher quantity of RANKL in scaffold lysates on western blot. Of note, for both OPG and RANKL, higher molecular weight species were also found in higher quantities in MCGO, suggesting dimerized protein. Immunoprecipitation with anti-RANKL demonstrated pulldown of OPG for both CGO and MCGO, whereas OPG was not co-immunoprecipitated with a control antibody. For both scaffolds, monomeric OPG as well as higher molecular species forms were co-immunoprecipitated. Immunoprecipitation with anti-OPG similarly indicated that RANKL was also pulled down in both CGO and MCGO lysates. Again, both monomeric RANKL and higher molecular weight species were found. However, monomeric RANKL was more efficiently co-immunoprecipitated in MCGO scaffold lysates, which may be secondary to the overall higher quantities of OPG that MCGO scaffolds carry compared to CGO.

Osteogenic Differentiation on MCGO

Next, we evaluated the functional effects of MCGO on osteogenic and osteoclast differentiation. Primary hMSCs were cultured on MC-GAG and MCGO scaffolds for 8 weeks and assessed for mineralization (Figure 4). Compared to cell-free MC-GAG scaffolds (Empty), both MC-GAG and MCGO demonstrated mineralization at 8 weeks with no differences between the two scaffolds. Comparison of the viability of hMSCs cultured on MC-GAG and MCGO using WST-1 analyses also revealed no significant

differences between the two materials (Figure 4B). In addition to mineralization on micro-CT, expression of differentiation markers was assessed (Figure 4C-E). No differences between MC-GAG and MCGO were seen in the expression of bone differentiation markers including ALP, COL1A1, OCN, BSP2, and RUNX2. Similarly, expression of BMP ligands and cartilage differentiation markers were similar between the two materials. In combination, these data suggest that OPG-functionalized (MCGO) scaffolds behave similarly to conventional MC-GAG scaffolds regarding osteogenic differentiation of hMSCs.

Osteoclastogenic Differentiation in Co-Cultures with MCGO

In contrast to hMSCs, viability and differentiation of primary human osteoclasts (hOCs) was severely reduced in the presence of both MC-GAG and MCGO scaffolds. Primary human osteoclasts cultured with MC-GAG or MCGO in osteoclastogenic differentiation medium supplemented with RANKL and M-CSF demonstrated a reduction in viability and proliferation on WST-1 analysis in comparison to control (Col-GAG) scaffolds (Figure 5A). Notably, MCGO scaffolds elicited a greater inhibition of osteoclast proliferation and viability compared to conventional MC-GAG variants.

To assess the differences in differentiation of primary hOCs in the presence of the different scaffolds, hOCs were stained with anti-TRAP, phalloidin to label F-actin, and Dapi to label nuclei (Figure 5B). In the presence of control (Col-GAG) scaffolds, large, multinucleated TRAP-positive cells were seen with actin ring formation, suggestive of differentiation of hOCs. hOCs cultured in the presence of MC-GAG demonstrated smaller, multinucleated TRAP-positive cells. Actin ring formation was found in some, but not all cells. In contrast to control scaffolds, more mononucleated TRAP positive cells compared to multinucleated cells were visualized, suggestive of a reduction in differentiation. In the presence of MCGO, a reduction in cells overall was found compared to control and MC-GAG scaffolds. Multinucleated TRAP positive cells were infrequently found on MCGO and were relatively diminutive in size.

To understand the overall effect of MCGO on mature osteoclast activity as well as in the presence of two simultaneously differentiating cell types, resorption was evaluated next (Figure 5C-D). Co-cultures of pre-osteoclasts with control (Col-GAG), MC-GAG, and MCGO materials were differentiated with and without hMSCs for 10 days on culture plates coated with inorganic crystalline calcium phosphate. Qualitative and quantitative characterization of resorption pit areas demonstrated significant differences among the different conditions [$F(4,27)=82.78$, $p<0.001$]. Among all scaffold types, control materials generated the highest resorptive activity at 97.54±3.39% with significant differences compared to all other conditions. Compared to MC-GAG, MCGO demonstrated a lower resorption (26.19±7.50% vs 75.92±11.10%, $p<0.0001$). In the presence of hMSCs simultaneously undergoing differentiation, MCGO continued to demonstrate lower rates of resorption compared to MC-GAG (27.99±4.10% vs 58.62±16.09%, $p<0.001$). These data suggested that MCGO scaffolds inhibit osteoclast maturation and resorption in isolation as well as in the presence of osteoprogenitors undergoing osteogenic differentiation within the scaffold microenvironment.

Mineralization of Rabbit Calvarial Defects Reconstructed with MCGO

Given the effects of MCGO on osteoclast inhibition *in vitro*, we next evaluated the potential for improvement in calvarial regeneration *in vivo* (Figure 6). 14 mm in diameter biparietal skull defects in 6-8 week old New Zealand white rabbits were unreconstructed (empty) or reconstructed with MC-GAG or MCGO materials. After 12 weeks, explanted skulls were evaluated for bone healing.

The explanted skulls were first assessed with micro-CT scanning to evaluate the amount of mineralization within the defects (Figure 6A-B). Qualitatively, an improvement in mineralization was visible in skulls reconstructed with MCGO compared to MC-GAG or unreconstructed defects. Quantification of the amount of mineralized content was derived using the median gray values from the micro-CT scan within a fixed volume of the defect internally corrected by the density within a fixed volume in the native calvarium for each animal to generate Defect/Native mineralization ratios. Defect/Native mineralization was then compared using a Kruskal-Wallis test and found to exhibit significant differences among the scaffolds [$H(2)=165.48$, $p<0.001$]. Both MC-GAG [median(IQR): 0.34(0.16)] and MCGO [median(IQR): 0.41(0.13)] exhibited significantly higher mineralization ratios compared to unreconstructed (empty) defects [median(IQR): 0.30(0.12), $p<0.0001$ and $p<0.001$, respectively]. In addition, MCGO reconstructed defects displayed a significantly higher defect/native mineralization ratio compared to MC-GAG reconstructed defects.

Histologic analyses of explanted cranial defects were also performed to confirm the presence of mineralization (Figure 6C). The unreconstructed, empty defects displayed largely fibrous, non-mineralized soft tissue within the defect. In contrast, both MC-GAG and MCGO reconstructed demonstrated more trabecular, mineralized content within the defects, albeit less organized than the surrounding native bone. Compared to MC-GAG, MCGO reconstructed defects demonstrated a greater overall thickness of both regenerated bone and residual soft tissue within the defect compared to empty defects, likely secondary to the thickness of the implanted scaffold. Quantification of the area of regenerated bone in relationship to the total area within the defect confirmed differences between the three conditions [$F(2,6)=17.34$, $p=0.003$]. Pairwise comparisons showed that MCGO displayed a higher ratio of bone area to defect area compared to empty ($p=0.003$) and MC-GAG-reconstructed defects ($p=0.02$) (Figure 6D). In combination, the micro-CT and histologic analyses suggested that MCGO was more efficient at mineralization compared to MC-GAG scaffolds.

Properties of Regenerated Rabbit Calvarium

The mechanical properties of the defect were next evaluated using reference point indentation with the surrounding native calvarium as an internal control for each rabbit (Figure 7). All bioindentation measurements were expressed as a relative ratio between defect to native bone in order to control for differences in bone healing and bone thickness between animals.

Two measures of strength were evaluated. The 1st cycle indentation distance (ID1st), a measure of hardness which is inversely correlated to mineralization and density, was found

to be significantly different among the groups [H(2)=51.30, p<0.001]. Both MC-GAG [median(IQR): 1.74(0.70)] and MCGO [median(IQR): 1.65(0.58)] exhibited significantly lower relative ID1st values compared to defect only controls [median(IQR): 2.49(1.74), p<0.001]. Comparison of the relative ID1st values between MCGO and MC-GAG demonstrated that MCGO was also significantly lower than MC-GAG (p=0.03).

The total indentation distance (TID), inversely correlated to microfracture resistance, was also found to be different among the groups [H(2)=47.88, p<0.001]. Similar to ID1st, both MC-GAG [median(IQR): 1.80(0.72)] and MCGO [median(IQR): 1.61(0.63)] demonstrated lower TID compared to defect only controls [median(IQR): 2.51(1.95), p<0.001]. MCGO also demonstrated lower values when compared to MC-GAG (p=0.02).

Average relative unloading slope (US) and loading slope (LS), measurements of stiffness, were also found to be significantly different among the groups [H(2)=16.37, p<0.001; H(2)=17.55, p<0.001, respectively]. In both measurements, MC-GAG and MCGO were significantly higher than defect only controls. However, no significant differences were found between MC-GAG and MCGO.

Discussion

In this work, we describe the fabrication and characterization of an osteoprotegerin-eluting nanoparticulate mineralized collagen glycosaminoglycan scaffold for skull regeneration. Our *in vitro* analyses indicated that the method of fabrication yielded a scaffold that eluted soluble OPG at earlier timepoints (day 0-14) than typical endogenous OPG production in primary human mesenchymal stem cells cultured on MC-GAG materials. In addition, the concentrations of eluted OPG in MCGO materials during days 0-14 mirrored that of concentrations produced by endogenous OPG from hMSCs at later timepoints. Minimal to no differences were seen between secreted OPG in hMSCs cultured on MC-GAG and MCGO beyond the first 14 days of culture, suggesting that MCGO imparted only a short-term increase in OPG within the surrounding microenvironment. However, the temporal increase in OPG significantly altered the overall OPG/RANKL equilibrium such that hMSCs cultured on MCGO displayed elevated OPG/RANKL ratios compared to MC-GAG or control scaffolds (Col-GAG) during the first 14 days of culture. The relative increase in soluble OPG to RANKL molar ratios paralleled scaffold-bound binding affinities of OPG on MCGO to purified RANKL. In an *in vitro* co-culture system, the functional consequences of OPG-elution by MCGO were confirmed with inhibition of pre-osteoclast activation via both TRAP staining and resorption pit analysis in a manner that exceeded the effects of MC-GAG, which has an intrinsic inhibitory effect on osteoclast maturation. When MCGO was evaluated for rabbit skull defect reconstruction, bone regeneration within the defect was found to be greater than MC-GAG and empty defect controls via both quantification of radiographic mineralized volumes within the defect as well as bone area in relationship to defect area on histology. Evaluation of the biomechanical properties of the MCGO-regenerated skulls showed a significant increase in both hardness and resistance to microfracture, but not stiffness, compared to MC-GAG-regenerated skulls. Altogether, these data suggest that a composite MC-GAG scaffold with OPG eluting capabilities improves skull regeneration via a transient downregulation of osteoclast maturation and activation.

Several other groups have explored the idea of incorporating OPG in regenerative strategies. Similar to our previous work using adenoviral-delivery of OPG to mesenchymal stem cells cultured on MC-GAG [20], Liu and colleagues reported that rat bone marrow stromal cells overexpressing OPG seeded on hydroxyapatite scaffolds improved healing of mandibular defects in an osteoporotic rat model [34]. Similarly, Su and colleagues showed that OPG overexpression in rabbit periodontal ligament stem cells (PDLSCs) cultured on beta-tricalcium phosphate materials improved regeneration of alveolar defects [35]. However, there are substantial disadvantages in reliance on adenoviral-mediated OPG delivery. First, the inability to control the quantity or conclusion OPG overexpression may be a potential downside as osteoclast-mediated bone remodeling would be prevented or delayed. Both our group and Liu et al have observed high levels and long-lasting OPG expression using adenoviruses such that the latter group reported a 5-6 fold reduction of osteoclast numbers compared to controls at 8 weeks following implantation [34]. Second, the delivery modality requires the addition of cells, thereby increasing the level of complexity and risk in translating the technology to the clinical realm. While regenerative, off-the-shelf materials for intraoperative use may provide a more favorable risk/benefit ratio compared to current clinically available options for skull reconstruction, cell-based therapies would introduce a significant increase in time consumption, cost, potential morbidity from progenitor cell harvest, and uncertain long-term effects. Due to the generally non-life-threatening nature of skull defects, cell-based approaches are unlikely to outweigh the drawbacks of the current clinical options.

With respect of composite materials, Jayash and colleagues have reported on the development of a chitosan gel with recombinant OPG [36–38]. Two differences between this material and the current report deserves mention. First, the release kinetics of the chitosan/OPG material suggested a longer period of release of beyond 30 days in *in vitro* culture, albeit the investigators evaluated total soluble protein in solution rather than the ELISA studies used in the current report. Second, the quantity of OPG elution ranged from 2-12 μg/mL with a starting concentration of 1 mg/mL of OPG for fabrication of the chitosan/OPG material, both of which are much higher concentrations than we have observed for endogenous soluble OPG production by differentiating hMSCs. The importance of temporal release as well as quantity of OPG as part of the composite material remains unclear at the moment. The biomechanical analyses in the current work demonstrated differences in strength of the mineralized content when comparing MCGO versus MC-GAG, while no differences in stiffness of the bone were demonstrated. These findings suggested that MCGO confers an advantage, however, further refinement to potentially increase the amount of OPG or to increase the length of time for OPG elution should be evaluated. Despite these considerations, the requirement for osteoclast activity in remodeling bone suggests that a temporal endpoint for osteoclast inhibition is necessary.

One of the major benefits in utilizing OPG as part of a regenerative strategy is the lack of signaling abilities, in contrast to growth factor delivery as the clinical risks of the latter have been well-documented. Within the spinal fusion literature, BMP-2 use has decreased since 2007 due to complications including heterotopic ossification, protracted pain, and osteolysis, suggestive that delivery of anabolic substances is clinically precarious [39, 40]. However, it is unknown whether delivery of a relatively inert, decoy receptor over a short period of time

in a defined local space would generate untoward effects. Within the literature, the role of osteoprotegerin as part of disease pathogenesis has been described in several arenas. Genetic polymorphisms of OPG have been reported in association with osteoporotic fractures as well as in otosclerosis, highlighting the clinical consequences of OPG deficiencies [41, 42]. In cancer, OPG is frequently elevated particularly in the setting of bone metastasis. However, OPG is generally considered a physiologic response to skeletal destruction rather than a contributor of pathology, such that downregulation of OPG by certain cancers such as multiple myeloma has been associated with lytic bone disease [43, 44]. The clinical consequences of OPG delivery will likely lack clarity until large-scale translation occurs with long-term data available.

An emerging condition-specific theme within our investigations on MC-GAG and the development of second-generation materials based on MC-GAG is derived from the observation that regenerative strategies must be tailored to the specific circumstances that define the clinical problem. While treatment of life-threatening illnesses may accept high risk therapies including those carrying significant complications, non-life-threatening conditions such as skeletal defects cannot and should not accept therapies that may risk greater harm or incur greater cost. Within skeletal defects, a variety of anatomic and functional differences also exist that preclude the ability to apply one type of regenerative technology to all defects. For example, in the craniofacial skeleton alone, defects of the alveolus must be reconstructed in a manner that can bear weight whereas the skull must be reconstructed in a manner that can withstand the lack of weight bearing and its ramifications on bony resorption. At the current time, MCGO has only been evaluated in the context of skull defect models and, thus, will require further consideration for suitability to other types of defects.

Conclusions

Our current work describes the fabrication, *in vitro*, and *in vivo* testing of an osteroprotegerin-eluting nanoparticulate mineralized collagen glycosaminoglycan material. The improvement in rabbit skull defect healing by MCGO compared to MC-GAG suggests that OPG composites may be further explored as a basis for skull regenerative materials.

Supplementary Material

Refer to Web version on PubMed Central for supplementary material.

Funding:

This work was supported by the National Institutes of Health/National Institute of Dental and Craniofacial Research under award numbers R01 DE029234 (JCL), R01 DE028098 (JCL), R01 DE030491 (BACH), the Bernard G. Sarnat Endowment for Craniofacial Biology (JCL), and the Jean Perkins Foundation (JCL). We are also grateful for funds provided by the NSF Graduate Research Fellowship (DGE-1746047 to VK; DGE-1144245 to MJD) and the Chemistry-Biology Interface Research Training Program at the University of Illinois (T32 GM070421, VK). We wish to acknowledge Siavash Jalal, PhD from the Office of Advanced Research Computing in the UCLA Institute of Digital Research and Education for statistical consultation.

References

[1]. Dewan MC, Rattani A, Fieggen G, Arraez MA, Servadei F, Boop FA, Johnson WD, Warf BC, Park KB, W.w.l.t.t.t.f.i.f.t.d.a.c.t.i.t.g.n.d.C.a.l.i.a. order:, J Neurosurg (2018) 1–10.

[2]. Hagan M, Bradley JP, J Craniofac Surg 28 (2017) 1129–1130. [PubMed: 28582309]

[3]. Sveikata L, Vasung L, El Rahal A, Bartoli A, Bretzner M, Schaller K, Schnider A, Leemann B, Neurosurg Rev 45 (2022) 1431–1443. [PubMed: 34618250]

[4]. Tarr JT, Hagan M, Zhang B, Tanna N, Andrews BT, Lee JC, Bradley JP, Plast Reconstr Surg 145 (2020) 1486–1494. [PubMed: 32195855]

[5]. Lee JC, Kleiber GM, Pelletier AT, Reid RR, Gottlieb LJ, Plastic and Reconstructive Surgery 132 (2013) 967–975. [PubMed: 24076686]

[6]. Tessier P, Kawamoto H, Posnick J, Raulo Y, Tulasne JF, Wolfe SA, Plast Reconstr Surg 116 (2005) 72S–73S; discussion 92S-94S. [PubMed: 16217446]

[7]. Zins JE, Langevin CJ, Nasir S, J Craniofac Surg 21 (2010) 1755–1760. [PubMed: 21119415]

[8]. Szpalski C, Wetterau M, Barr J, Warren SM, Tissue Eng Part B Rev 18 (2012) 246–257. [PubMed: 22029448]

[9]. Lee JC, Volpicelli EJ, Adv Healthc Mater (2017).

[10]. Lee JC, Pereira CT, Ren X, Huang W, Bischoff D, Weisgerber DW, Yamaguchi DT, Harley BA, Miller TA, J Craniofac Surg (2015).

[11]. Ren X, Bischoff D, Weisgerber DW, Lewis MS, Tu V, Yamaguchi DT, Miller TA, Harley BA, Lee JC, Biomaterials 50 (2015) 107–114. [PubMed: 25736501]

[12]. Ren X, Tu V, Bischoff D, Weisgerber DW, Lewis MS, Yamaguchi DT, Miller TA, Harley BA, Lee JC, Biomaterials 89 (2016) 67–78. [PubMed: 26950166]

[13]. Weisgerber DW, Caliari SR, Harley BA, Selective addition of mineral into collagen scaffolds to enhance hMSC osteogenesis and matrix remodeling, Acta Biomaterialia, 2014.

[14]. Weisgerber DW, Caliari SR, Harley BA, Biomater Sci 3 (2015) 533–542. [PubMed: 25937924]

[15]. Ren X, Weisgerber DW, Bischoff D, Lewis MS, Reid RR, He TC, Yamaguchi DT, Miller TA, Harley BA, Lee JC, Adv Healthc Mater 5 (2016) 1821–1830. [PubMed: 27275929]

[16]. Zhou Q, Ren X, Bischoff D, Weisgerber DW, Yamaguchi DT, Miller TA, Harley BAC, Lee JC, Adv Healthc Mater 6 (2017).

[17]. Zhou Q, Lyu S, Bertrand AA, Hu AC, Chan CH, Ren X, Dewey MJ, Tiffany AS, Harley BAC, Lee JC, Macromol Biosci (2020) e2000370. [PubMed: 33382197]

[18]. Zhou Q, Ren X, Oberoi MK, Bedar M, Caprini RM, Dewey MJ, Kolliopoulos V, Yamaguchi DT, Harley BAC, Lee JC, Adv Healthc Mater 10 (2021) e2101467. [PubMed: 34585526]

[19]. Ren X, Zhou Q, Foulad D, Dewey MJ, Bischoff D, Miller TA, Yamaguchi DT, Harley BAC, Lee JC, J Tissue Eng Regen Med (2019).

[20]. Ren X, Zhou Q, Foulad D, Tiffany AS, Dewey MJ, Bischoff D, Miller TA, Reid RR, He TC, Yamaguchi DT, Harley BAC, Lee JC, Sci Adv 5 (2019) eaaw4991. [PubMed: 31206025]

[21]. Takegahara N, Kim H, Choi Y, Bone 159 (2022) 116353. [PubMed: 35181574]

[22]. Maxhimer JB, Bradley JP, Lee JC, Genes Dis 2 (2015) 57–68. [PubMed: 25961069]

[23]. Anderson DM, Maraskovsky E, Billingsley WL, Dougall WC, Tometsko ME, Roux ER, Teepe MC, DuBose RF, Cosman D, Galibert L, Nature 390 (1997) 175–179. [PubMed: 9367155]

[24]. Kong YY, Yoshida H, Sarosi I, Tan HL, Timms E, Capparelli C, Morony S, Oliveira-dos-Santos AJ, Van G, Itie A, Khoo W, Wakeham A, Dunstan CR, Lacey DL, Mak TW, Boyle WJ, Penninger JM, Nature 397 (1999) 315–323. [PubMed: 9950424]

[25]. Yun TJ, Tallquist MD, Aicher A, Rafferty KL, Marshall AJ, Moon JJ, Ewings ME, Mohaupt M, Herring SW, Clark EA, J Immunol 166 (2001) 1482–1491. [PubMed: 11160187]

[26]. Simonet WS, Lacey DL, Dunstan CR, Kelley M, Chang MS, Lüthy R, Nguyen HQ, Wooden S, Bennett L, Boone T, Shimamoto G, DeRose M, Elliott R, Colombero A, Tan HL, Trail G, Sullivan J, Davy E, Bucay N, Renshaw-Gegg L, Hughes TM, Hill D, Pattison W, Campbell P, Sander S, Van G, Tarpley J, Derby P, Lee R, Boyle WJ, Cell 89 (1997) 309–319. [PubMed: 9108485]

[27]. Harley BA, Leung JH, Silva ECCM, Gibson LJ, Acta Biomaterialia 3 (2007) 463–474. [PubMed: 17349829]

[28]. Harley BA, Lynn AK, Wissner-Gross Z, Bonfield W, Yannas IV, Gibson LJ, Journal of Biomedical Materials Research. Part A 92 (2010) 1066–1077. [PubMed: 19301274]

[29]. Weisgerber DW, Kelkhoff DO, Caliari SR, Harley B.a.C., Journal of the Mechanical Behavior of Biomedical Materials 28 (2013) 26–36. [PubMed: 23973610]

[30]. Olde Damink LH, Dijkstra PJ, van Luyn MJ, van Wachem PB, Nieuwenhuis P, Feijen J, Biomaterials 17 (1996) 765–773. [PubMed: 8730960]

[31]. Tiffany AS, Dewey MJ, Harley BAC, RSC Adv 10 (2020) 26982–26996. [PubMed: 33767853]

[32]. Schindelin J, Arganda-Carreras I, Frise E, Kaynig V, Longair M, Pietzsch T, Preibisch S, Rueden C, Saalfeld S, Schmid B, Tinevez J-Y, White DJ, Hartenstein V, Eliceiri K, Tomancak P, Cardona A, Nature Methods 9 (2012) 676–682. [PubMed: 22743772]

[33]. Gallant MA, Brown DM, Organ JM, Allen MR, Burr DB, Bone 53 (2013) 301–305. [PubMed: 23274349]

[34]. Liu X, Bao C, Xu HHK, Pan J, Hu J, Wang P, Luo E, Acta Biomaterialia 42 (2016) 378–388. [PubMed: 27318268]

[35]. Su F, Liu SS, Ma JL, Wang DS, E LL, Liu HC, Stem Cell Res Ther 6 (2015) 22. [PubMed: 25888745]

[36]. Jayash SN, Hashim NM, Misran M, Baharuddin NA, PeerJ 4 (2016) e2229. [PubMed: 27635307]

[37]. Jayash SN, Hashim NM, Misran M, Baharuddin N, Journal of Biomedical Materials Research Part A 105 (2017) 398–407. [PubMed: 27684563]

[38]. Jayash SN, Hashim NM, Misran M, Baharuddin NA, PeerJ 5 (2017) e3513. [PubMed: 28674665]

[39]. Cahill KS, Chi JH, Day A, Claus EB, JAMA 302 (2009) 58–66. [PubMed: 19567440]

[40]. Lord EL, Cohen JR, Buser Z, Meisel HJ, Brodke DS, Yoon ST, Youssef JA, Wang JC, Park JB, Global Spine J 7 (2017) 603–608. [PubMed: 28989837]

[41]. Priyadarshi S, Ray CS, Biswal NC, Nayak SR, Panda KC, Desai A, Ramchander PV, Ann Hum Genet 79 (2015) 225–237. [PubMed: 25998045]

[42]. Langdahl BL, Carstens M, Stenkjaer L, Eriksen EF, J Bone Miner Res 17 (2002) 1245–1255. [PubMed: 12096838]

[43]. Honore P, Luger NM, Sabino MA, Schwei MJ, Rogers SD, Mach DB, O'keefe PF, Ramnaraine ML, Clohisy DR, Mantyh PW, Nat Med 6 (2000) 521–528. [PubMed: 10802707]

[44]. Seidel C, Hjertner Ø, Abildgaard N, Heickendorff L, Hjorth M, Westin J, Nielsen JL, Hjorth-Hansen H, Waage A, Sundan A, Børset M, Group NMS, Blood 98 (2001) 2269–2271. [PubMed: 11568016]

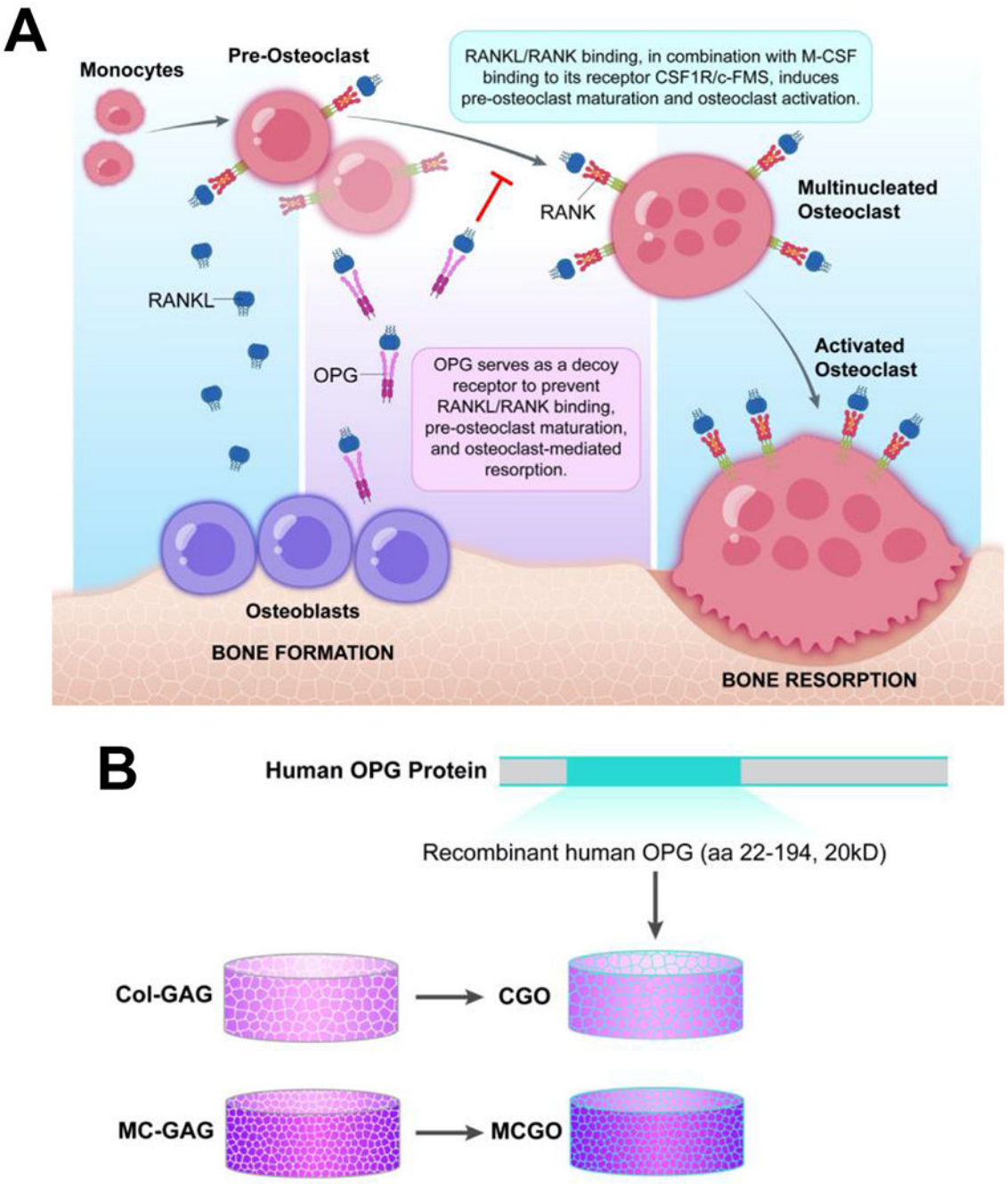

Figure 1. OPG Activity and Scaffold Fabrication

(A) Model of endogenous OPG activity in inhibition of osteoclast maturation and activation. **(B)** Schematic of non-mineralized (CGO) and mineralized (MCGO) fabrication and functionalization with recombinant human OPG.

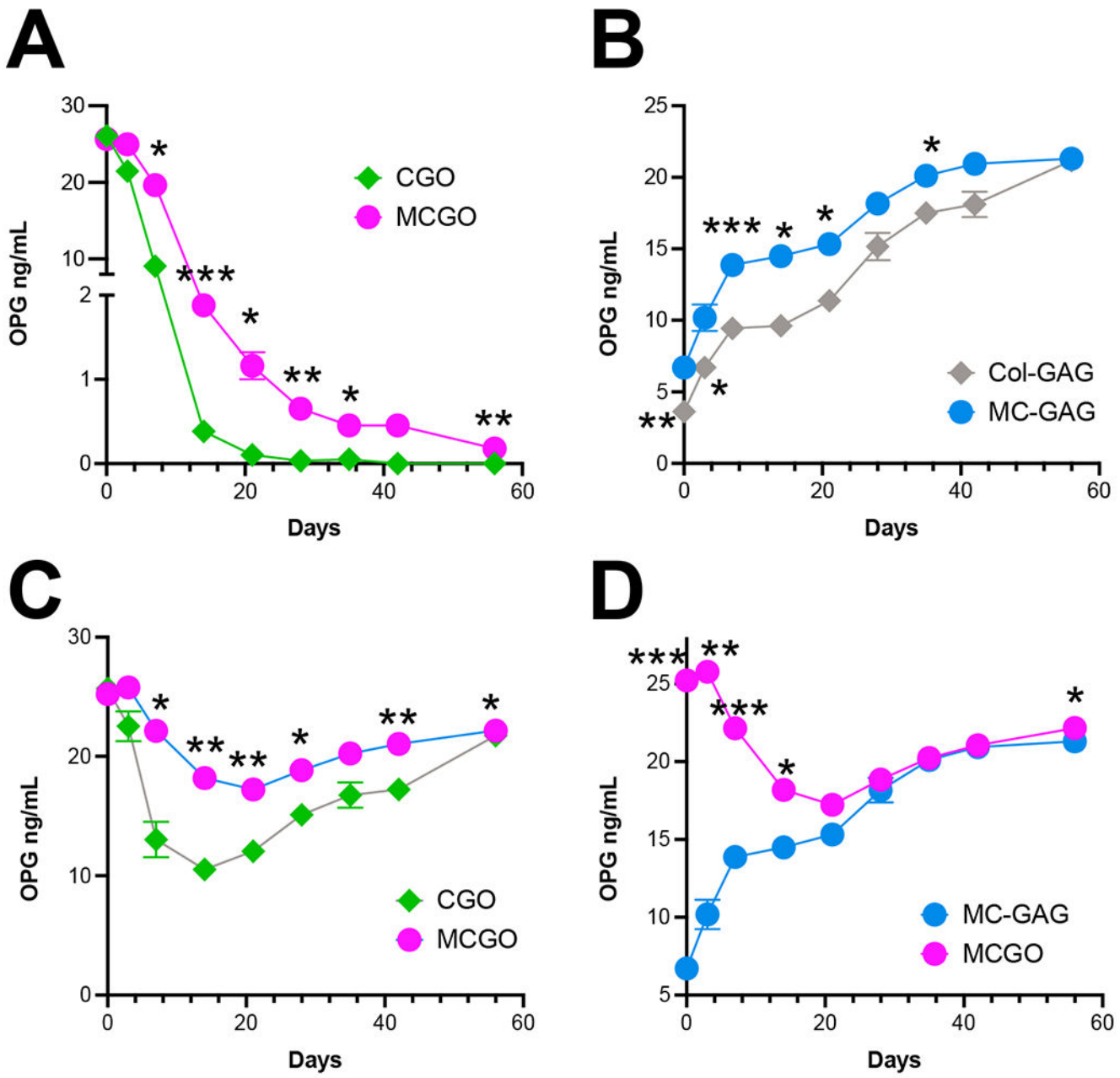

Figure 2. Scaffold-mediated OPG Elution and Endogenous Soluble OPG Secretion.

ELISA for soluble OPG (ng/mL) from cultures over 8 weeks of: **(A)** CGO and MCGO cell-free scaffolds, **(B)** hMSCs cultured on Col-GAG and MC-GAG scaffolds, **(C)** hMSCs cultured on CGO and MCGO scaffolds, and **(D)** hMSCs cultured on MC-GAG and MCGO scaffolds. Corresponding tables with estimated marginal means (EM Means) with 95% Confidence Intervals (95% CI) OPG concentrations of each scaffold type at the specified days in culture in Supplementary Tables 2–4. Error bars display SE. Representative images and analyses from two independent experiments with n=3-4 per timepoint. Asterisks denote significant comparisons between the scaffold pairs at each timepoint. *, $p<0.05$; **, $p<0.01$; ***, $p<0.001$.

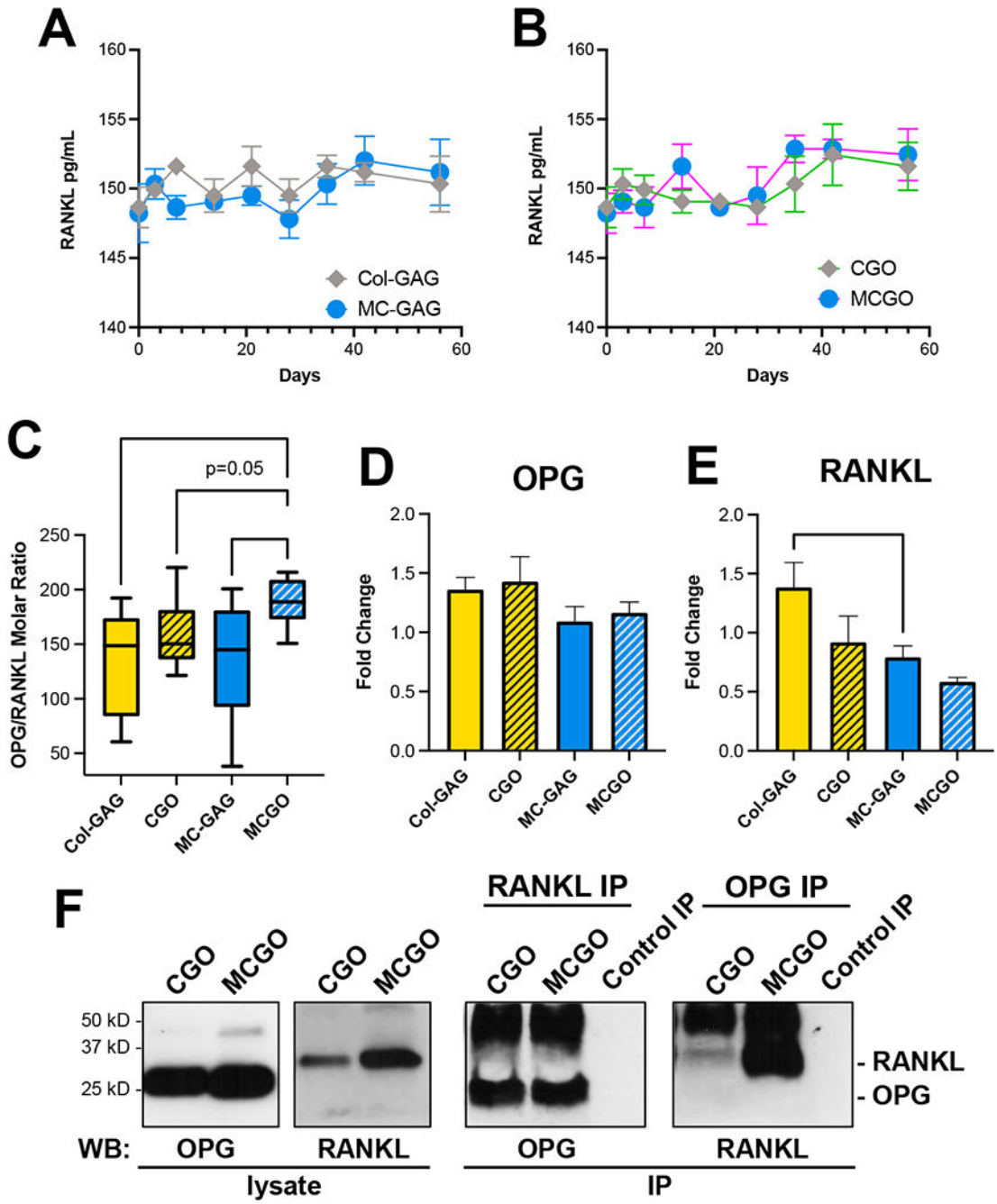

Figure 3. OPG and RANKL Relative Molar Ratios, Gene Expression, and Binding Affinities on OPG-Eluting Scaffolds

ELISA for soluble RANKL from cultures over 8 weeks of: **(A)** primary hMSCs differentiated on Col-GAG and MC-GAG and **(B)** primary hMSCs differentiated on CGO and MCGO. **(C)** Molar ratios of soluble OPG and RANKL from ELISA over the first 14 days of culture expressed using Tukey box and whisker plots. Quantitative data analyzed using Kruskal-Wallis tests with pairwise comparisons using Dunn's test with Bonferroni adjustments. QPCR for (**D**) OPG or (**E**) RANKL in primary hMSCs cultured on Col-GAG,

CGO, MC-GAG, or MCGO for 7 days (n=4-8). Quantitative data analyzed using ANOVA with pairwise comparisons under the Tukey criterion. **(F)** Co-immunoprecipitation with cell-free CGO or MCGO and purified RANKL protein using anti-RANKL (RANKL IP), anti-OPG (OPG IP), or anti-rabbit control antibodies (Control IP). Lysates prepared from each of the scaffolds (left panels) and immunoprecipitates (IP, right panels) were then western blotted (WB) for OPG or RANKL as indicated. *, $p<0.05$; **, $p<0.01$.

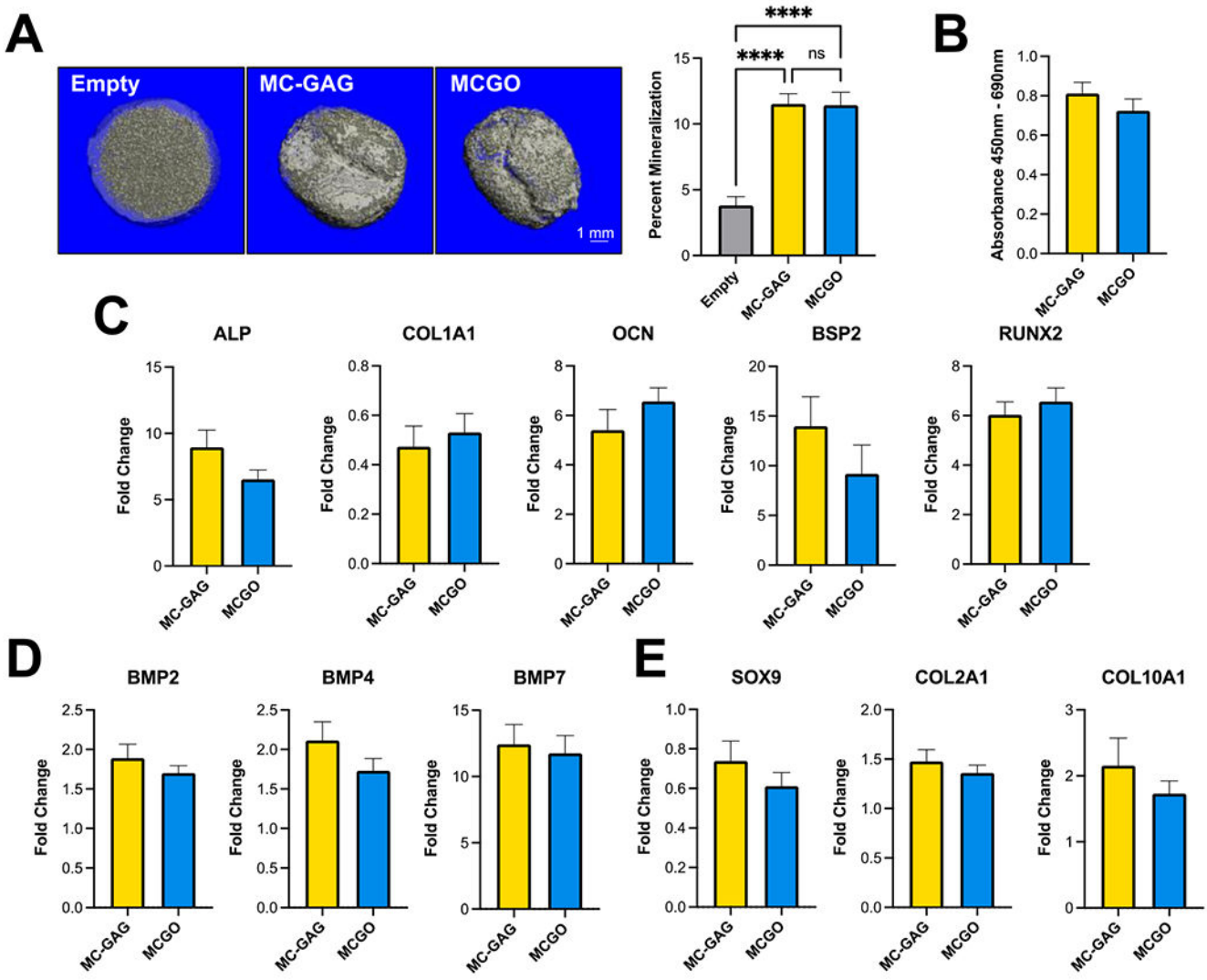

Figure 4. Effect of MC-GAG and MCGO on Osteogenic Differentiation

(**A**) Cell-free MC-GAG (Empty) and primary hMSCs cultured on MC-GAG or MCGO for 8 weeks were subjected to micro-CT. Representative images and quantification of percent mineralization are shown. (**B**) WST-1 analysis of hMSCs cultured on MC-GAG or MCGO for 8 weeks. QPCR for (**C**) osteogenic differentiation markers (ALP, COL1A1, OCN, BSP2, RUNX2), (**D**) BMP ligand expression (BMP2, BMP4, BMP7), and (**E**) chondrogenic differentiation markers (SOX9, COL2A1, COL10A1) in primary hMSCs cultured on MC-GAG or MCGO for 7 days (n=8). Quantitative data assessed using student's t test for two groups and ANOVA with posthoc comparisons under the Tukey criterion for data with 3 groups. *, $p<0.05$; ****, $p<0.0001$.

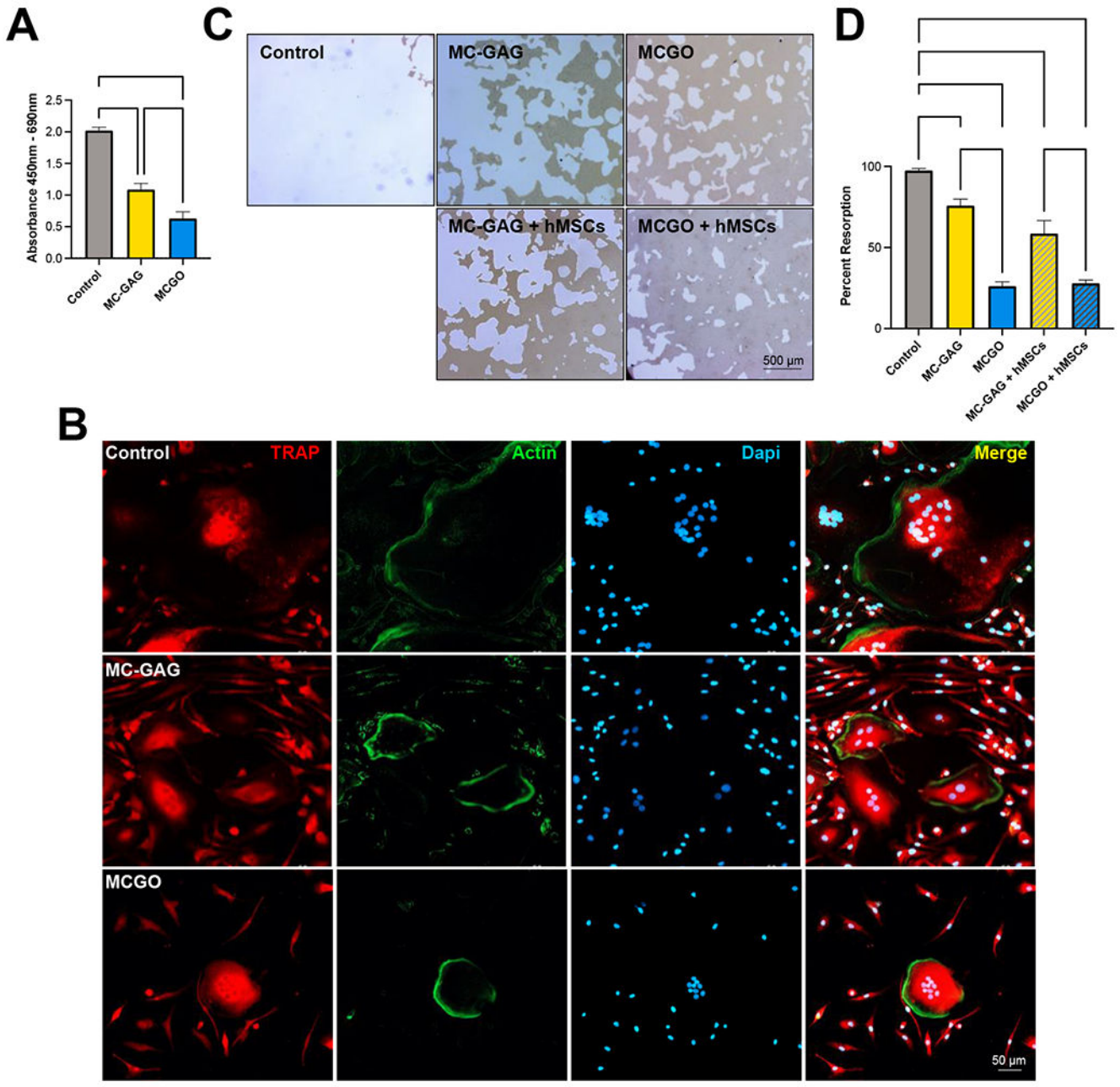

Figure 5. Effect of MC-GAG and MCGO on Osteoclast-Mediated Resorption in Co-Cultures

(**A**) WST-1 analysis and (**B**) immunofluorescent microscopy of hOCs cultured with control (Col-GAG), MC-GAG, or MCGO for 10 days in osteoclastogenic differentiation medium. Anti-TRAP (red), phalloidin (green), Dapi (blue), and merged representative images are shown. Data presented from 3–4 independent experiments. Representative images from four independent experiments (**C**) and quantitative analysis (**D**) of resorption pit assays of co-cultures of pre-osteoclasts cultured with Control (Col-GAG), MC-GAG, MC-GAG with hMSCs, MCGO, and MCGO with hMSCs for 10 days in combined osteogenic

and osteoclastogenic medium. Quantitative data assessed using ANOVA with posthoc comparisons under the Tukey criterion. *, $p<0.05$; ***, $p<0.001$.

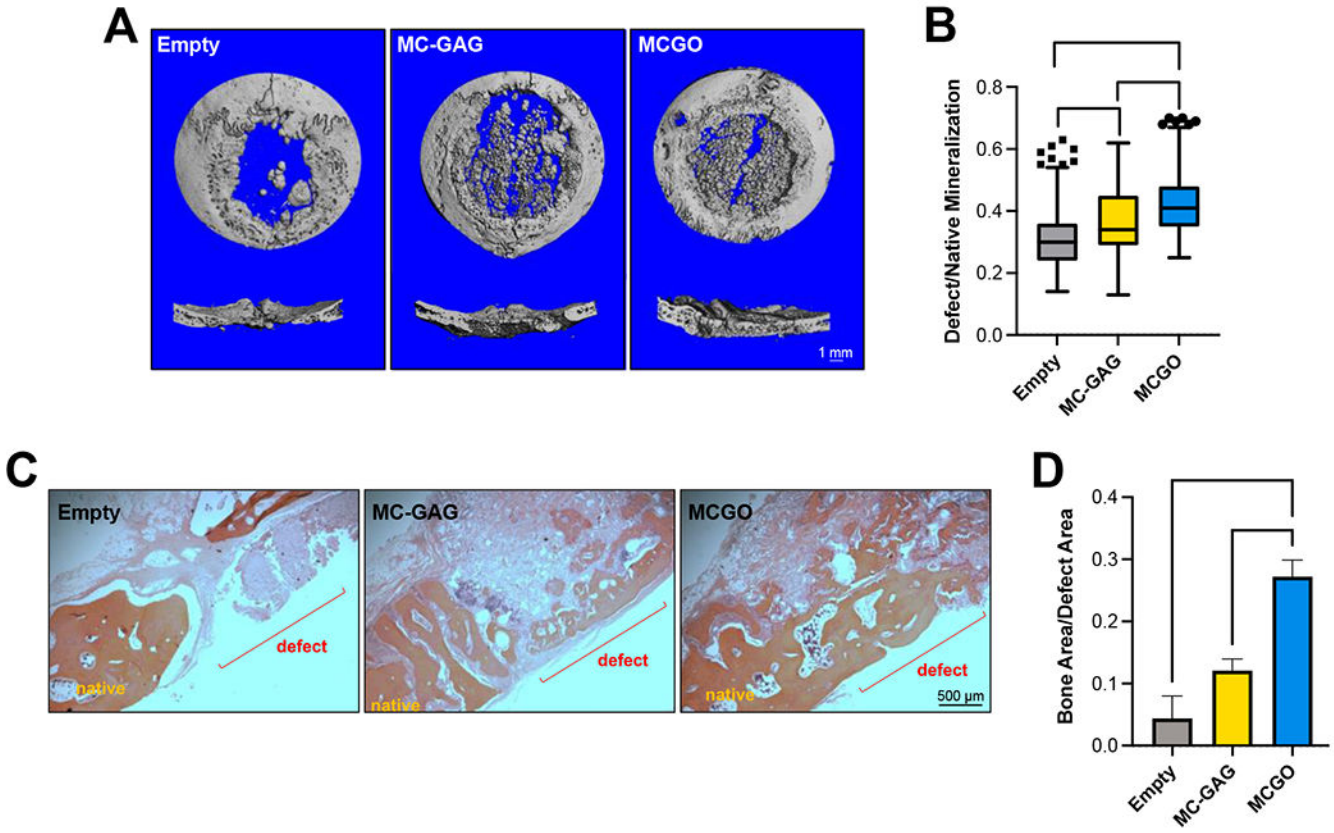

Figure 6. In Vivo Rabbit Calvarial Regeneration in Skull Defects Implanted with MC-GAG and MCGO

Representative images (A) and quantitative analysis (B) of micro-CT scanning of explanted rabbit skulls 12 weeks after creation of 14 mm biparietal skull defects without reconstruction (Empty) or with reconstruction using MC-GAG or MCGO. Quantitative data expressed as a ratio of mineralization within the defect corrected by mineralization within the surrounding native bone using Tukey box and whisker plots. Quantitative data analyzed using Krukal-Wallis tests with pairwise comparisons using Dunn's test with Bonferroni adjustments. Representative images (C) and quantitative analysis (D) of H&E staining of histologic sections within rabbit cranial defects explanted after 12 weeks. Quantitative data expressed as a ratio of mineralization within the defect corrected by mineralization within the surrounding native bone. Quantitative data analyzed using ANOVA with pairwise comparisons under the Tukey criterion. *, $p<0.05$; **, $p<0.01$; ***, $p<0.001$.

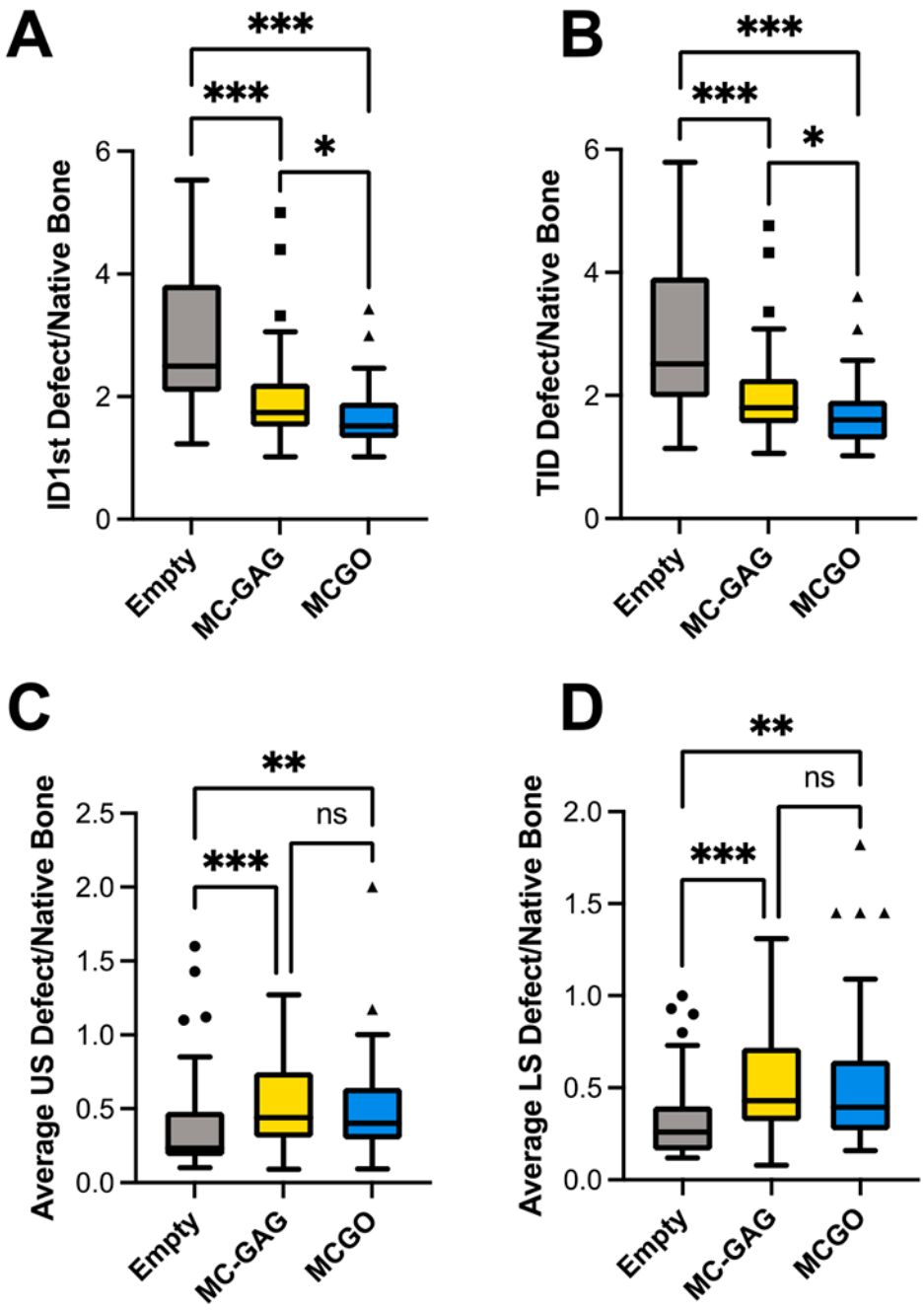

Figure 7. Biomechanical Properties of Rabbit Skull Defects Reconstructed with MC-GAG and MCGO

Reference point indentation in explanted rabbit skulls with 14 mm biparietal calvarial defects unreconstructed (Empty) or reconstructed with MC-GAG or MCGO for 12 weeks showing (**A**) first cycle indentation distance (ID1st), (**B**) total indentation distance (TID), (**C**) unloading slope (US), and (**D**) loading slope (LS). All measurements were expressed as a ratio of the defect to native bone to account for individual differences in biomechanical

properties within specific animals using Tukey box and whisker plots. *, $p<0.05$; **, $p<0.01$; ***, $p<0.001$.